Multiplex surface-enhanced Raman scattering identification and quantification of urine metabolites in patient samples within 30 min

Kao, Ya-Chuan; Han, Xuemei; Lee, Yih Hong; Lee, Hiang Kwee; Phan-Quang, Gia Chuong; Lay, Chee Leng; Sim, Howard Yi Fan; Phua, Vanessa Jing Xin; Ng, Li Shiuan; Ku, Chee Wai; Tan, Thiam Chye; Phang, In Yee; Tan, Nguan Soon; Ling, Xing Yi

2020

Kao, Y.-C., Han, X., Lee, Y. H., Lee, H. K., Phan-Quang, G. C., Lay, C. L., ... Ling, X. Y. (2020). Multiplex surface-enhanced Raman scattering identification and quantification of urine metabolites in patient samples within 30 min. ACS Nano, 14(2), 2542-2552. doi:10.1021/acsnano.0c00515

https://hdl.handle.net/10356/143412

https://doi.org/10.1021/acsnano.0c00515

Multiplex Surface-Enhanced Raman Scattering Identification and Quantification of Urine Metabolites in Patient Samples within 30 Minutes

Ya-Chuan Kao,[1] Xuemei Han,[1] Yih Hong Lee,[1] Hiang Kwee Lee,[1] Gia Chuong Phan-Quang,[1] Chee Leng Lay,[1,5] Howard Yi Fan Sim,[1] Vanessa Jing Xin Phua,[1] Li Shiuan Ng,[1] Chee Wai Ku,[4] Thiam Chye Tan,[4] In Yee Phang,[5] Nguan Soon Tan,[2,3,] Xing Yi Ling[1,*]*

Address

[1] Division of Chemistry and Biological Chemistry, School of Physical and Mathematical Sciences, Nanyang Technological University, 21 Nanyang Link, Singapore 637371, Singapore.

[2] Lee Kong Chian School of Medicine, Clinical Sciences Building, Nanyang Technological University, 11 Mandalay Road, Singapore 308232, Singapore.

[3] School of Biological Sciences, Nanyang Technological University, 60 Nanyang Drive, Singapore 637551, Singapore.

[4] KK Women's and Children's Hospital, 100 Bukit Timah Road, Singapore 229899, Singapore.

[5] Institute of Materials Research and Engineering, Agency for Science, Technology and Research (A*STAR), 2 Fusionopolis Way, Innovis, #08-03, Singapore 138634, Singapore.

E-mail: NSTan@ntu.edu.sg; xyling@ntu.edu.sg

Abstract. Successful translation of laboratory-based surface-enhanced Raman scattering (SERS) platforms to clinical applications requires multiplex and ultratrace detection of small metabolites from a complex biofluid. However, these metabolites exhibit low Raman scattering cross-sections and do not possess specific affinity to plasmonic nanoparticle surfaces, significantly increasing the challenge of detecting them at low concentrations. Herein, a 'confine-and-capture' approach is demonstrated for multiplex detection of two families of urine metabolites correlated with miscarriage risks, 5β-pregnane-3α,20α-diol-3α-glucuronide and tetrahydrocortisone. To enhance SERS signals by 10^{12}-fold, specific nanoscale surface chemistry is used for targeted metabolite capture from a complex urine matrix prior to confining them on a superhydrophobic SERS platform. Applying chemometrics, including principal component analysis and partial least square regression, enables conversion of molecular fingerprint information into quantifiable readouts. The whole screening procedure requires only 30 minutes, including urine pretreatment, sample drying on the SPHB-mirror platform, SERS measurements and chemometric analyses. These readouts correlate well with the pregnancy outcomes in a case-control study of 40 patients presenting threatened miscarriage symptoms.

Keywords. surface-enhanced Raman spectroscopy (SERS), superhydrophobic SERS platform, chemometrics, metabolomics, urine-based diagnostic test

Achieving ultratrace detection of small molecules with low Raman scattering cross-sections and without specific affinity to plasmonic nanoparticle surfaces remains challenging in surface-enhanced Raman scattering (SERS) spectroscopy.[1-3] This difficulty is further compounded by the need to perform multiplex and quantitative molecular detection from a complex matrix. Successfully addressing these issues is instrumental towards the translating laboratory-based SERS platforms into practical sensing devices.[4] SERS offers multiple advantages over conventional analytical platforms such as fluorescence-based techniques.[5] SERS platforms can be tailored to generate intense electromagnetic field enhancements and dense plasmonic hotspots, in turn enhancing molecule-specific Raman vibrational fingerprint intensities by $>10^9$-fold.[6,7] These fingerprints exhibit substantially narrower peak widths as compared to the broad fluorescence emission bands (full-width half-maximum of ~ 2 nm *versus* 30 nm respectively), further enabling SERS to achieve label-free multiplex analysis with ease.[8] SERS measurements also require significantly shorter time as compared to conventional chromatography- or mass spectrometry-based analytical approaches, whereby SERS analyses can be completed within an hour.[9] More importantly, the fingerprint specificity of SERS readouts enables differentiation of isomeric structures which cannot be easily achieved using other techniques.[10-12] However, majority of current SERS research focus predominantly on platform design, using standard molecules with large Raman scattering cross-sections or molecules with specific affinity to plasmonic nanoparticle surfaces as proof-of-concept analytes to showcase the platform's capability to attain high SERS enhancement factors.[13-17] This focus inadvertently creates a gap in the trace detection of small molecules which are omnipresent in the aforementioned practical scenarios.[18-20] To overcome this bottleneck, new detection strategies which venture beyond hotspot engineering are required.

Herein, we demonstrate rapid and ultrasensitive SERS screening of small metabolites with low Raman scattering cross-sections from a complex biofluid. We utilize a two-pronged 'confine-and-capture' strategy to efficiently generate the strongest SERS signal enhancement for our target metabolites. To confine metabolites, we design a plasmonic-active superhydrophobic SERS platform to physically concentrate analytes into a ~185-fold smaller area as compared to a hydrophilic substrate. To selectively capture our target metabolites from a urine matrix, we graft Ag nanocubes with a self-assembled monolayer of capturing agent which preferentially reacts with the metabolites through covalent interactions. Our strategy generates an analytical SERS enhancement factor (AEF) of 10^{12}. We further employ chemometric analysis to process large datasets across the entire measured spectral range, thereby enabling us to achieve quantitative multiplex screening of metabolites down to parts-per-trillion levels. (Scheme 1)

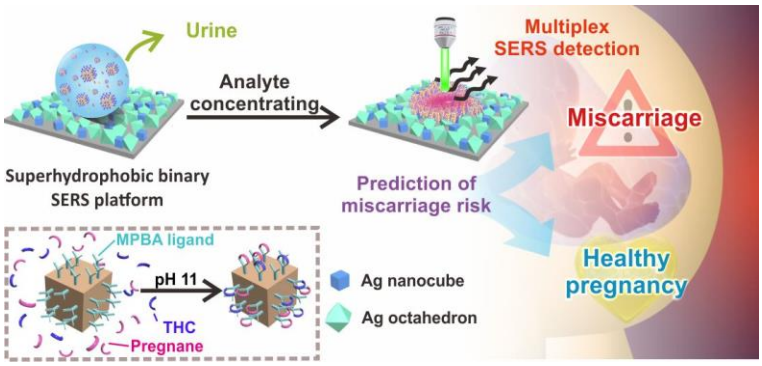

Scheme 1. Schematic illustration of our metabolomics-based SERS diagnostic platform to stratify miscarriage risk among pregnant women presenting symptoms of threatened miscarriage. We outline a confine-and-capture strategy for ultrasensitive metabolite screening: a superhydrophobic SERS platform physically confines metabolites on the platform and a probe molecule (4-mercaptophenylboronic acid, MPBA) selectively captures target metabolites from a complex urine matrix.

As our proof-of-concept, we perform a case-control study of 40 urine samples collected from pregnant women presenting with threatened miscarriage. Threatened miscarriage occurs in 15 – 20% of all pregnancies in the first trimester and is characterized by abdominal pain or vaginal bleeding; 25% of these pregnancies progress to suffer spontaneous miscarriage.[21] There is currently a lack of non-invasive point-of-care diagnostic platform for clinicians to predict miscarriage risks among patients exhibiting symptoms of threatened miscarriage at the point of care. Among various biomarkers investigated in meta-analysis, serum progesterone has been proposed as a useful clinical biomarker to predict the risk of miscarriage.[21-23] A low serum progesterone level < 35 nmol/L has been proposed as high risk for spontaneous miscarriage.[21,24] However, clinical serum progesterone measurement is invasive and requires time-consuming laboratory-based test using progesterone chemiluminescence immunoassay kit. Consequently, the diagnostic utility of this test is limited as a clinical management decision needs to be made on the spot. More importantly, the predictive power of single serum progesterone suffers from low diagnostic accuracy due to their wide range of fluctuations. Hence, it is important to use a combination of biomarkers to increase the accuracy of diagnosis.[25,26]

A recent metabolomic investigation of threatened miscarriage using patient urine samples reveals a panel of metabolites, which can serve as potential biomarkers for non-invasive diagnosis of spontaneous miscarriage.[27] In particular, there is a positive correlation between the risk of spontaneous miscarriage and the relative abundance of two metabolites from the progesterone and cortisol families: 5β-pregnane-3α,20α-diol-3α-glucuronide (pregnane) and tetrahydrocortisone (THC). Liquid chromatography-mass spectrometry (LC-MS) shows that pregnane% ≥ 98.7% (relative pregnane/THC ratio of 76/1) corresponds to an ongoing pregnancy, whereas pregnane%

≤ 97.4% (relative ratio of 38/1) corresponds to a spontaneous miscarriage. However, LC-MS analysis generates semi-quantitative results, requires long screening time, and has limited sensitivity, thus hindering the use of metabolomics for point-of-care risk stratification for spontaneous miscarriage.

To quantify the relative concentrations of these two metabolites from patient samples with known pregnancy outcomes, we successfully correlate SERS readouts with miscarriage risks among the patients within 30 minutes. Our ability to detect metabolites from patient samples at ultra-trace levels implies the potential application of our SERS platform as non-invasive point-of-care screening technology for other diseases and conditions in the broad field of metabolomics.

Results and discussion

In the first step of our 'confine-and-capture' strategy, we fabricate a superhydrophobic (SPHB) SERS substrate using a binary mixture of monodisperse Ag nanocubes and octahedra. Both nanocubes and octahedra exhibit > 95 % shape purity post-purification. The well-defined tips generate intense electromagnetic field enhancements, and their size difference creates high surface roughness essential to achieve superhydrophobicity (edge length = 128 ± 7 and 299 ± 22 nm; Figure S1). We employ electrostatic assembly to fabricate the SERS platform, functionalizing Ag building blocks with negatively charged 11-mercaptoundecanoic acid (11-MUA) and Si substrate with positively charged amino groups (Figure 1A). After assembly, we perform ligand exchange on the platform with perfluorodecanethiol (PFDT) and coat it with an additional Ag adhesive layer to create a stable superhydrophobic plasmonic nanostructured surface (Figure S2).[28] This adhesive

layer is also essential to prevent possible particle re-dispersion from the substrate surface in the subsequent addition of liquid analyte droplets.[26]

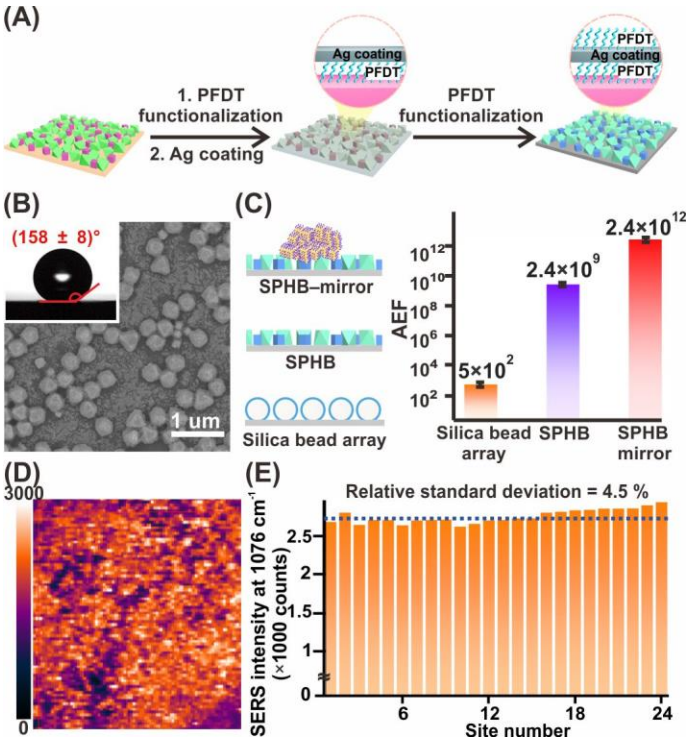

Figure 1. (A) Fabricating SPHB SERS platform using nanocubes and octahedra. (B) Static water contact angle and SEM image of the optimized SPHB platform. (C) Comparing AEFs between SPHB-mirror, SPHB, and silica bead array, to elucidate the relative contribution of analyte concentrating effects and electromagnetic field enhancements to the overall observed AEF on our SERS platform. Error bars in (C) are s.d. of 25 measurements. (D) Hyperspectral SERS intensity distribution map of one featured C=C vibrational mode of methylene blue (1628 cm^{-1}) using our SPHB platform, which demonstrates a good signal reproducibility and homogeneity of the platform. (E) Homogeneous intensity profile of the methylene blue peak at 1630 cm^{-1} peak on the SPHB substrate.

Our electrostatic self-assembly approach enables us to make use of particle ratio and assembly immersion time to optimize the surface hydrophobicity of our platform. Using a 1:4 ratio of nanocubes to octahedra, we achieve an optimized SPHB platform with a particle density of (4.4 ± 0.2) particles/μm^2 and a static water contact angle of (158 ± 8) ° (Figure 1B, Figures S3 and S4). This platform exhibits the highest surface roughness of (116 ± 6) nm, which is 1.3- and 1.2-fold higher than the surface roughness of platforms formed using uniform nanocubes or octahedra under identical experimental conditions respectively (Figure S5). To quantify the analyte concentrating factor of the SPHB platform, we compare the dried surface contact area of a 1 µL silica bead aqueous solution on our SPHB platform and a hydrophilic Si substrate (contact angle < 20°). The contact area of the silica beads on the SPHB platform is ~ 0.13 mm^2, 185-fold smaller than the 24 mm^2 spot area on the hydrophilic Si substrate (Figure S5). These physical characterizations of the SPHB platform indicates effective confinement of a liquid droplet into a small contact area (Figures S6 and S7), which is essential to boost sensitivity towards the subsequent SERS detection of trace metabolites.

To quantify the SERS enhancement capabilities of the SPHB platform, we systematically study the AEF using the C=C vibrational mode of methylene blue at 1628 cm^{-1}.[12] We compare the analytical SERS enhancement factor (AEF) of the silica bead-based superhydrophobic substrate with our Ag-layer coated binary Ag particles-based SERS substrate. Both substrates are superhydrophobic (SPHB). The AEF for non-plasmonic active silica beads array is calculated to be 5×10^2 (Figure S8), whereas the AEF of our superhydrophobic binary SERS substrate is estimated to be 2.4×10^9 (Figure 1C). We acknowledge that the SERS enhancement of the silica bead-based substrate (5×10^2) may arise from the Ag layer coating and the superhydrophobicity

of the substrate to concentrate the analyte into small area. By comparing these two substrates, we minimize the potential differences arising from the concentrating effect from SPHB surface. The additional 4.8×10^6-fold enhancement in our SPHB SERS substrates is mainly attributed to the presence of hot spots on and between the Ag nanocubes and octahedra.[6,7] These results further demonstrate the need of plasmonic nanocrystals as building block is clearly evident.

To further increase the AEF of our platform to 2.4×10^{12} for ultrasensitive metabolite detection, with a detection limit down to 10^{-14} M and an analytical dynamic range from 10^{-4} to 10^{-14} M. we mix the analytes with a dispersion of Ag nanocubes with fixed concentration, and subsequently drop cast the mixture onto the SPHB platform. This approach further boosts the AEF by 10^3-fold relative to the SPHB platform (Figure 1C and Figure S8). This signal enhancement arises from two additional effects. Trapping the analytes among the dispersion of Ag nanocubes significantly increases hotspot densities, and the subsequent introduction of the analyte-Ag nanocubes dispersion to the SPHB platform creates a "mirror effect" between the additional nanocubes and the SPHB SERS-active surface.[29-31] More importantly, our platform exhibits highly consistent SERS intensities. SERS spectra extracted across a hyperspectral SERS map of a dried droplet demonstrate similar spectral features, with good signal reproducibility and homogeneity (relative standard deviation of 4.5%; Figures 1D and 1E). As such, our subsequent experiments will be conducted using this "SPHB-mirror" modality.

In the second step of our 'confine-and-capture' strategy, we graft the Ag nanocubes dispersion with a self-assembled monolayer of 4-mercaptophenylboronic acid (MPBA; Figure 2A). MPBA functions as probes to selectively capture our target metabolites, pregnane and THC, from the urine matrix *via* the formation of boronate ester bond under alkaline conditions.[32-38] This bond localizes the metabolites near the plasmonic nanoparticle surfaces for maximum SERS enhancement.[39,40] A

direct detection approach in which the metabolites are simply mixed with the plasmonic nanoparticles prior to SERS measurements does not work, because these metabolites have very weak Raman-scattering cross-sections.

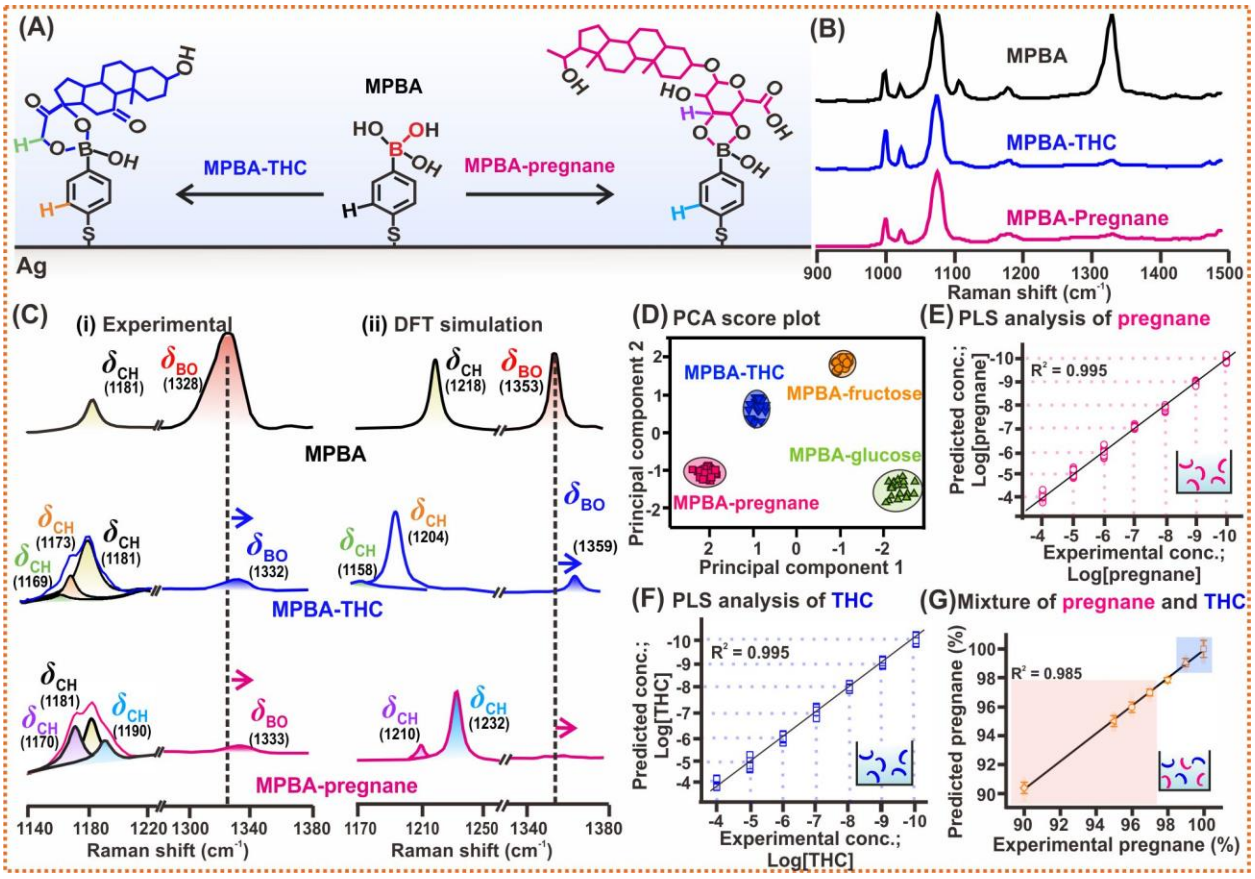

Figure 2. (A) Interaction of MPBA with pregnane and THC on the Ag nanocubes' surface. (B) SERS spectra of MPBA, MPBA-THC and MPBA-pregnane. (C) Key spectral changes involving boronate ester moiety at 1140 to 1380 cm^{-1} in the presence of pregnane and THC. (i) Experimental measured SERS spectra and (ii) DFT simulated SERS spectra of MPBA, MPBA-pregnane and MPBA-THC. (D) Controlled experiment of 4-MPBA with pregnane, THC, fructose and glucose. The PCA result shows that 4-MPBA molecules have high specificity for pregnane and THC molecules. (E), (F) PLS analyses of concentration-dependent SERS spectra of pregnane and THC from 10^{-4} M to 10^{-10} M, respectively. (G) PLS analysis of a mixture comprising pregnane and THC

with different pregnane%. Ongoing pregnancy and miscarriage regions are highlighted in blue and pink, respectively. Error bars in (f) are s.d. of 25 measurements.

To investigate the SERS spectral changes arising from the chemical interactions between MPBA and the metabolites, we react MPBA-functionalized Ag nanocubes with aqueous pregnane or THC (10^{-4} M), and drop cast 10 µL of the reaction mixture onto our SPHB platform for SERS measurements (Figure 2B). The SERS spectrum of neat MPBA-grafted nanocubes exhibit two characteristic vibrational modes at 1181 and 1328 cm^{-1} (Figure 2C).[41] In the presence of THC, the 1328 cm^{-1} band intensity decreases sharply with a concomitant blue-shift to ~1332 cm^{-1} (Figure 2Ci). Two new peaks are also observed at 1169 and 1173 cm^{-1} near the peak at 1181 cm^{-1}. Similarly, in the presence of pregnane, we note an intensity decrease and blue-shift of 1328 cm-1 band to ~1333 cm^{-1} and emergence of two new peaks at 1170 and 1190 cm^{-1}. These spectral changes in vibrational fingerprints before and after interaction with the metabolites are direct evidence of the interaction between the metabolites and MPBA-functionalized nanocubes.

To elucidate the molecular origin of the observed spectral changes, we employ density functional theory (DFT) to simulate the SERS spectra of MPBA and that of MPBA bound individually to pregnane and THC, (Figure 2Cii), respectively. Our model comprises a MPBA molecule on the apex of Ag6 cluster (Ag-MPBA). The distinct vibrational modes of MPBA at 1181 and 1328 cm^{-1} are indexed to C-H bending from benzene ring (δ_{CH}) and bending mode of boronic acid (δ_{BO}), respectively.[42,43] We then place the metabolites separately near Ag-MPBA, and allow the system to relax to form the complex structure. For MBPA-THC, the C-H vibration mode shift from 1218 cm^{-1} to lower position at 1204 cm^{-1} and 1158 cm^{-1}, whereas for MBPA-pregnane, the C-H vibration mode shift from 1218 cm^{-1} toward higher wavenumbers at 1232 cm^{-1} and another new C-H mode appear at lower position at 1210 cm^{-1}. Notably, in our experiments, the Ag surface

grafted MBPA molecules are not fully reacted with the metabolites, thus the experimental spectrum can arise from a mixed spectrum of unreacted MPBA and those reacted with metabolites. In both cases, the chemical interactions of THC and pregnane with MPBA lead to a significant decrease in peak intensity of the δ_{BO} bending at ~1328 cm^{-1}, and a concomitant blue shift. The formation of the boronate ester bond restricts B-O bond vibration and reduces the bond polarizability, thereby resulting in a higher energy requirement for B-O bond vibration. In the presence of THC, the experimentally observed SERS peaks at 1169 and 1173 cm^{-1} can be indexed to C-H bending mode (δ_{CH}) in the boronate ester moiety (Table S1). Similarly, for pregnane-MPBA, C-H bending mode is also observed at 1170 and 1190 cm^{-1} in the experimental spectra.[41,43] Collectively, these results affirm the strong chemical interaction of MPBA with both pregnane and THC, enabling the potential SERS quantification of these metabolites.

To achieve speedy and accurate metabolite identification which are important for the stratification of miscarriage risk in clinical settings, we apply principal component analysis (PCA) to our data. PCA extracts key information across the entire spectral range measured while simultaneously eliminating noise and reducing human errors.[44] We apply standard normal variate correction and Savitzky-Golay derivative algorithm as data pretreatment to a total of 75 SERS spectra corresponding to MPBA, MPBA-THC, and MPBA-pregnane, respectively, prior to the unsupervised clustering process.

These spectra are individually collected under the same experimental conditions using a laser beam with an excitation wavelength of 532 nm and laser power of 0.2 mW with spectral acquisition time of 1 s. 25 SERS spectra from each group, corresponding to a total of 75 spectra, are selected randomly without any specific criteria for analysis since our platform exhibit good signal homogeneity. These 75 SERS spectra are loaded without any background correction, using a total

of 6 loading vectors for PCA analysis. For PCA score plotting, PC1 and PC2 account for a respective 81.89 % and 15.18 % of the variance in the SERS spectra we analyzed. Hence, the sum of PC1 and PC2, *etc.* 97.07% indicates that almost all the variables observed in the SERS spectra can be accounted for. The output data along PC1 demonstrates three distinct clusters, each corresponding to MPBA, MPBA-pregnane and MPBA-THC, indicating that they can be differentiated unambiguously (Figures S9A, S10). We further demonstrate the capability to distinguish the metabolites' SERS signals from the SERS signals of common sugars such as glucose and fructose (Figure 2D and Figure S9B). These sugars are possible interferences that could be present in various biofluids and they interact similarly with MPBA. Our results thus highlight how integrating PCA with our 'confine-and-capture' strategy can effectively extract relevant SERS spectral variations with high specificity.

Next, we employ partial least square regression (PLS) to establish a standard calibration curve for our metabolites and to predict the analyte concentrations by computing 210 SERS spectra from 10^{-4} M to 10^{-10} M (Figure 2E, 2F, and Figure S9).[45] PLS regression plots the experimental metabolite concentration on the x-axis and the predicted metabolite concentration on the y-axis. Our calibration curve shows a near-ideal linearity spanning 7 orders of magnitude, with linear coefficients of 0.995 and 0.994 for MPBA-pregnane and MPBA-THC, respectively. Hence, PLS can construct a good prediction model based on concentration-dependent changes across the entire experimentally measured spectral window, notably within a very short time frame (< 5 min). This statistically robust model is certainly unachievable through manual data analyses, where the signal intensities of specific fingerprints at different concentrations are individually collated and could easily be subject to human errors.

We further conduct multiplex detection using a mixture of pregnane and THC following similar sample preparation and SERS measurement conditions as previously described. We use pregnane% to define the relative metabolite concentrations in a multiplex setup, and is calculated using ([pregnane])/([THC]+[pregnane]). The total amount of the mixture (pregnane+THC) is kept constant at 0.1 nM, in accordance to the potential relative metabolite abundance in patient urine samples.[27] Previous LCMS studies have revealed that pregnane% ≥ 98.7% (relative pregnane/THC ratio of 76/1) corresponds to an ongoing pregnancy; whereas pregnane% ≤ 97.4% (relative ratio of 38/1) corresponds to a spontaneous miscarriage.[24] To build a quantification model to determine the relative abundance of pregnane/THC, we collect SERS spectrum of our MPBA reacted with a series of pregnane and THC mixture that have different percentage of pregnane by using non-pregnant women's urine samples. Typically, a pregnane% sample indicates there is 90% pregnane and 10% THC in the solution. The corresponding pregnane (THC) concentrations for pregnane% of 97.4% and 98.7% are 0.0974 nM (0.0026 nM) and 0.0987 nM (0.0013 nM) respectively. We further treat the collected SERS spectra using PLS to study the pregnane percentage by analyzing the peak disappearance and wavelength shift within whole spectra for MBPA after reacting with metabolites that have different percentage of pregnane. Multivariate PLS analysis will automatically resolve minor changes in metabolite among different concentrations in a multiplex setup comprising biofluids and construct the corresponding model for miscarriage risk determination. In our multiplex setup, the prediction model continues to display a high linear coefficient of 0.985 at various pregnane%, indicating that our SPHB-mirror platform gives rise to good predictive accuracy for the multiplex detection of metabolites (Figure 2G). We achieve superior detection sensitivity even with minor changes in the concentrations of two metabolites at ultratrace levels. These levels correspond to physiologically relevant concentrations, further

highlighting the potential applicability of our platform to screen for metabolites in biofluids.[18] In our experiments, we maintain a 400-fold excess of MPBA probes relative to the total metabolite concentration, thus allowing all target metabolites to be effectively captured. Notably, we also successfully extend our analytical approach to screen for our target urine metabolites in spiked artificial urine (Figure S11).

Next, we conduct a case-control study of 40 women who present with threatened miscarriage between 5 to 10 weeks of gestation at the emergency department of KK Women's and Children's Hospital (CIRB ref: 2013/320/D; Figure 3A). Urine specimens are collected at presentation. We classify women who subsequently had spontaneous miscarriages as cases (n = 20), and those with ongoing pregnancy at 16 weeks gestation as controls (n = 20). Differences in SERS spectral signatures are observable from these two patient groups (Figure 3B). To establish a calibration baseline for metabolite level quantification, we use urine specimens from non-pregnant women. All urine samples undergo a ZIPTIP pretreatment, which comprises an 18-carbon chain functionalized silica column (Figure S11B), to remove salt and water-soluble interferences (Scheme S1).[43] We react the MPBA functionalized Ag nanocubes with the metabolites at alkaline pH to facilitate the covalent bond formation. Before the reaction, we extract the metabolites from the biological urine sample using a standard micro-filtration product ZIP-TIP. Passing the urine through this micro-column will allow the relatively less polar urine metabolites to be adsorbed within the column. Rinsing the column first with water elutes any adsorbed ions from the system. Subsequent rinsing with methanol extracts the urine metabolites from the micro-column. Adding MPBA-functionalized Ag nanocubes into the eluent containing our urine metabolites at pH 11 allows selective analyte capture. Therefore, the pH of raw urine sample will not affect the subsequent SERS analysis. We spike the urine samples from non-pregnant women with various

pregnane% to build up the prediction model (Figure 3C and Figure S12). The linear coefficients of this PLS prediction model are higher than 0.99, signifying reliability of our method even among patient urine samples.

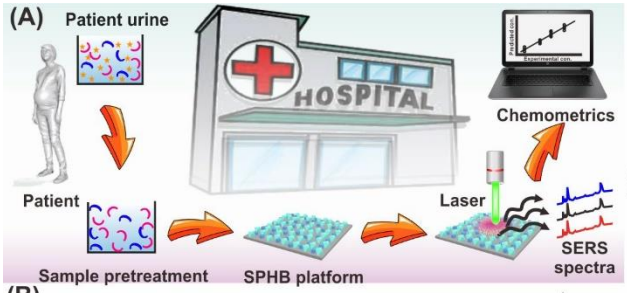

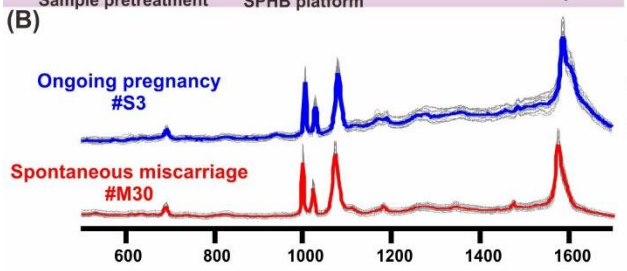

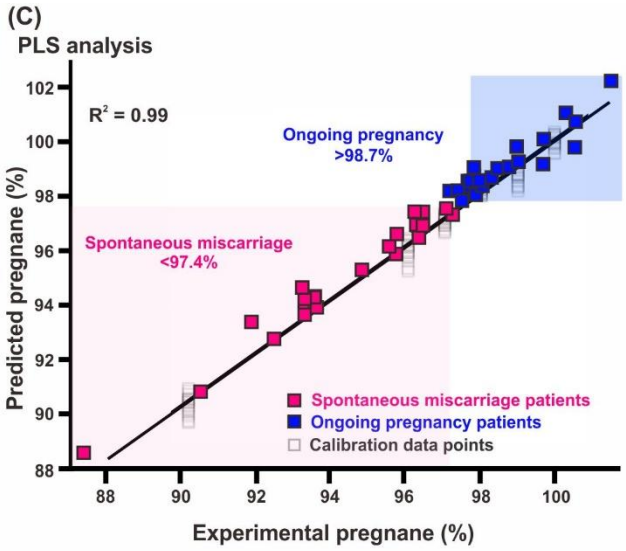

(D)

No.	LC-MS results (%)	SERS predicted results (%)	Absolute difference (%)	Outcome
S1	98.6	100.1 ± 0.3	1.5	Ongoing pregnancy
S2	98.8	99.2 ± 0.2	0.4	Ongoing pregnancy
S3	99.1	98.7 ± 0.4	0.4	Ongoing pregnancy
S4	99.0	102.3 ± 0.5	3.3	Ongoing pregnancy
S5	98.7	98.6 ± 0.4	0.1	Ongoing pregnancy
S6	99.3	101.1 ± 0.6	1.8	Ongoing pregnancy
S7	98.2	98.5 ± 0.2	0.3	Ongoing pregnancy
S8	98.7	99.1 ± 0.4	0.4	Ongoing pregnancy
S9	98.7	98.0 ± 0.3	0.7	Ongoing pregnancy
S10	99.0	99.0 ± 0.6	0.0	Ongoing pregnancy
S11	98.1	98.0 ± 0.2	0.1	Ongoing pregnancy
S12	98.7	97.9 ± 2.2	0.8	Ongoing pregnancy
S13	99.3	99.2 ± 0.2	0.1	Ongoing pregnancy
S14	99.4	98.3 ± 0.6	1.1	Ongoing pregnancy
S15	99.6	98.5 ± 0.7	1.1	Ongoing pregnancy
S16	98.2	98.0 ± 0.9	0.2	Ongoing pregnancy
S17	99.4	99.3 ± 0.1	0.1	Ongoing pregnancy
S18	99.6	100.7 ± 0.2	1.1	Ongoing pregnancy
S19	98.9	99.8 ± 0.6	0.9	Ongoing pregnancy
S20	98.9	99.1 ± 0.1	0.2	Ongoing pregnancy

No.	LC-MS results (%)	SERS predicted results (%)	Absolute difference (%)	Outcome
M21	87.7	88.6 ± 0.7	0.9	Miscarriage
M22	96.7	97.5 ± 0.2	0.8	Miscarriage
M23	97.2	96.0 ± 0.2	1.2	Miscarriage
M24	97.9	97.6 ± 0.2	0.3	Miscarriage
M25	98.2	97.4 ± 0.5	0.8	Miscarriage
M26	94.7	93.7 ± 0.2	1.0	Miscarriage
M27	97.2	95.3 ± 0.3	1.9	Miscarriage
M28	94.1	96.8 ± 0.4	2.4	Miscarriage
M29	93.1	92.4 ± 1.1	0.7	Miscarriage
M30	96.7	96.9 ± 0.4	0.2	Miscarriage
M31	98.8	97.3 ± 0.5	1.5	Miscarriage
M32	91.9	90.7 ± 0.3	1.2	Miscarriage
M33	95.1	94.1 ± 0.3	1.0	Miscarriage
M34	95.5	94.7 ± 0.8	0.8	Miscarriage
M35	92.7	93.4 ± 0.9	0.7	Miscarriage
M36	95.7	92.8 ± 0.3	2.9	Miscarriage
M37	96.7	96.6 ± 0.2	0.1	Miscarriage
M38	95.5	94.0 ± 0.4	1.5	Miscarriage
M39	95.8	96.7 ± 0.3	0.9	Miscarriage
M40	98.4	96.6 ± 0.6	1.8	Miscarriage

Figure 3. (A) Process of patient sample preparation, SERS screening and chemometric analysis. (B) Representative SERS spectra of urine samples collected from miscarriage patient number 30 and ongoing pregnancy patient number 3. (C) Building up PLS prediction model by mixing various pregnane% (10^{-10} M) with non-pregnant urine samples. Pregnane% from 20 ongoing pregnancy urine samples (blue squares) and 20 spontaneous miscarriage urine samples (pink squares). (D) Relative pregnane% measured from our SERS platform compared against LC-MS analyses for ongoing pregnancy samples (S1-S20) and miscarriage samples (M1-M20).

For the 40 patient samples presenting threatened miscarriage, we extract a minimum of 25 spectra for each patient sample for analysis. The SERS spectra are loaded into the prediction model for the quantification of metabolite levels. The metabolite levels obtained from our SPHB-mirror SERS platform show excellent correlation with those obtained *via* LC-MS analyses (Figure 3D). The absolute difference between SERS predicted pregnane% and LC-MS is 0.0 – 3.1%. This slight deviation may arise from the use of single measurements in the LC-MS analyses.

We successfully employ our SPHB-mirror platform to perform quantitative and multiplex metabolite detection in patient samples, notably at ultratrace levels using just 10 μL of urine. In our detection system, the whole screening procedure requires only 30 minutes, including urine pretreatment, sample drying on the SPHB-mirror platform, SERS measurements and chemometric analyses.[46,47] This detection method is faster than conventional LC-MS analyses, which can take several hours to days for urine profiling. This finding establishes our detection approach as a promising point-of-care tool for triaging the risk of spontaneous miscarriage in patients presenting with threatened miscarriage in a clinical setting.

Conclusions

In conclusion, we have developed a SERS platform which is capable of performing multiplex and ultrasensitive metabolite screening within 30 minutes to address current challenges of using SERS technique for sensing biomarkers such as metabolites. These metabolites exhibit low Raman scattering cross-sections and have no specific affinity towards plasmonic nanoparticle surfaces. Their low physiological abundance further exacerbates the difficulty in SERS detection, especially from a complex biological sample. By designing a confine-and-capture strategy, our binary superhydrophobic platform boosts SERS signals by 10^{12}-fold, thus enabling detection of metabolites at sub-nanomolar (parts-per-trillion) levels using just 10 µL of sample. Furthermore, PCA analyses enables us to elucidate spectral changes that arise upon the binding of urine metabolites with our capturing agent, thereby successfully identifying molecular fingerprints corresponding to the target metabolites and at the same time eliminate interferences that may be present in biological matrices. PLS analyses convert all molecular fingerprints across the entire spectral window into quantifiable SERS readouts, generating a linearity range spanning 7 orders of concentration changes. More importantly, PLS analyses can also pick up minor changes in metabolite concentrations at 0.1 nM levels in a multiplex setup comprising biofluids, thereby enabling us to apply our platform to quantitatively screen patient samples for key metabolites rapidly. Our SERS platform thus resolves various technical challenges that plague SERS substrates and restrict their translation into practical screening tools.

Using our platform, we can quantify both pregnane and tetrahydrocortisone levels among 40 pregnant women presenting symptoms of threatened miscarriage in a case-control study. Threatened miscarriage is one of the most common gynecological emergencies worldwide and there are currently no point-of-care screening tests to identify miscarriage risks. Clinicians

typically adopt a ‘watch-and-wait’ strategy or administer routine treatment with oral progestogens which may not be beneficial for all patients. Our non-invasive detection approach will significantly reduce undue distress among patients, and enable clinicians to administer prompt medical intervention. From a broader perspective, this combination of our SERS platform with metabolomics present multiple advantages over existing analytical platforms, including highly specific molecular fingerprinting for unambiguous metabolite identification, label-free multiplexing capabilities, ultralow sub-nanomolar detection limits (parts-per-trillion levels), straightforward sample treatment, low sample volume requirements, and non-invasive rapid quantification. Our approach can potentially be applied to screen for various diseases in numerous clinical settings, and is particularly useful where only small sample volumes are available for screening, such as tears or sputum.

Methods/Experimental

Chemicals. Silver nitrate ($AgNO_3$, ≥ 99%), anhydrous 1,5-pentanediol (PD, ≥ 97%), poly(vinylpyrrolidone) (PVP, average MW = 55000 g/mol), toluene (99.5%), 11-mercaptoundecanoic acid (MUA, 95%), 4-mercaptoboronic acid (MPBA, 90%), ammonia (28-30%), 1H,1H,2H,2H-perfluorodecanethiol (PFDT, 97+%), sodium chloride (NaCl, 99.5%), monopotassium phosphate (KH_2PO_4, 99%), glucose ($C_6H_{12}O_6$, ≥ 99.5%), fructose ($C_6H_{12}O_6$, ≥ 99%), and sodium phosphate (Na_3PO_4, 96%), were purchased from Sigma Aldrich; copper (II) chloride ($CuCl_2$, ≥ 98%), 3-aminopropyltriethoxysilane (APTES, 98%) were from Alfa Aesar; ethanol (ACS, ISO, Reag. Ph Eur) was from EMSURE; hydrochloric acid (HCl, 37%) was purchased from Analar Normapur. Tetrahydrocortisone (THC) was purchased from Scientific Resources. 5β-pregnane-3α,20α-diol-3α-glucuronide (pregnane) was purchased from AXIL

Scientific PTE LTD. All chemicals were used without further purification. Milli-Q water (>18.0 MΩ.cm) was purified with a Sartorius Arium 611 UV ultrapure water system.

Synthesis and purification of shape-controlled Ag polyhedra. The preparation process was carried out according to the polyol reduction method,[48] starting first with the synthesis of Ag nanocubes (AgNC). 20 mL PD was added to a 100 mL round bottom flask and heated to 190 ˚C for 10 minutes. Aliquots of 250 μL PVP and 500 μL AgNO3 precursor solutions were then alternately added to the reaction flask. This process was continued until the reaction mixture turned reddish brown. For the subsequent growth of Ag octahedra (AgNO), this solution was used without further treatment, using more concentrated precursor solutions. The reaction was allowed to proceed for ~2 h. The Ag polyhedra solutions were re-dispersed in 20 mL ethanol *via* multiple centrifugation rounds and purified through vacuum-filtration.

Ligand exchange reactions for Ag polyhedra. Ag polyhedra were separately functionalized with 11-MUA and MPBA through standard ligand exchange reactions. For 11-MUA functionalized Ag nanocubes (AgNCs), 1 mL ethanol was added to AgNC in ethanol suspension (0.1 mL, 2 mg mL^{-1}) and the supernatant was discharged after centrifugation. The AgNC were then re-dispersed in 1.5 mL of mixture of isopropyl alcohol (IPA) and ethanol with volume ratio of 1:1 under stirring speed of 500 rpm at 25 ˚C. Subsequently, 0.05 mL 11-mercaptoundecanoic acid (11-MUA) in IPA solution (0.1 mM) was added into the AgNC dispersion. The reaction mixture was then left for 4 hours at ambient condition and the supernatant was removed after centrifugation at 6500 rpm for 4.5 minutes. The same ligand replacement process was repeated once more. The AgNC colloidal suspension was then washed with copious amount of IPA and ethanol to remove excess 11-MUA. Finally, the AgNC were re-dispersed in 1.5 mL mixture of IPA and ethanol (volume ratio, 1:1) and stored under nitrogen gas protection for further use. Zeta

potential measurement was then carried out to measure the surface charges of AgNC. Similarly, the ligand exchange process was performed for AgNO colloidal solutions (0.1 mL, 13.7 mg/mL), using a solution of 11-MUA (0.1 mL, 10 mM) in IPA. Zeta potential measurements were then conducted using ZETASIZER NANO with DTS1070 folded capillary cell to measure the surface charges of the MUA functionalized Ag polyhedra.

For MPBA functionalized Ag nanocubes, 1 mL ethanol was added to AgNC in ethanol suspension (0.1 mL, 2 mg/mL) and the supernatant was discharged after centrifugation. The AgNC were then re-dispersed in 1.5 mL of mixture of isopropyl alcohol (IPA) and ethanol with volume ratio of 1:1 under stirring speed of 500 rpm at 25 ^{o}C. Subsequently, 0.05 mL MPBA in IPA solution (0.1 mM) was added into the AgNC dispersion. The reaction mixture was then left for 4 hours at ambient condition and the supernatant was removed after centrifugation at 6500 rpm for 4.5 minutes. The process was repeated once more, before repeating the same ligand reaction for a further 3 hours. The resulting solution was centrifuged, and supernatant was removed. The AgNC was then dispersed in 1.5 mL of IPA/ethanol (1:1, v/v), sonicated and centrifuged. The process was repeated twice, and the resulting product will be re-dispersed in 1 mL mixture of ethanol.

Surface functionalization of silicon wafer. Si wafer (1.5 cm × 1.5 cm) was subjected to oxygen plasma treatment for 5 minutes and then submerged in an anhydrous toluene solution containing 3-aminopropyltriethoxysilane (2 % in volume) for another 5 minutes. Subsequently, the amine-terminated Si wafer was rinsed with anhydrous toluene and methanol, followed by blow drying with N2 gas to remove any unfunctionalized ligands and solvents. The functionalized Si wafer was then submerged in an acid solution (pH= 5) for 5 minutes for further protonation of the amine-terminated wafer surface and render its surface positively-charged. The resulting platforms were kept in a nitrogen environment for further use.

Fabrication of binary superhydrophobic SERS chip. The binary superhydrophobic chip was fabricated by firstly submerging the positively charged Si substrates into 2 mL of 11-MUA functionalized Ag nanocubes and octahedra mixture solution for 20 minutes. The surface negatively charged Ag polyherdrals anchored on Si substrates surface *via* static interaction. The Ag polyhedra anchored Si substrates were then removed from the colloidal solution, rinsed with copious ethanol, and dried under nitrogen gas blowing. Such Si substrates were then coated with Ag layer (thickness of 25 nm) *via* thermal evaporation followed by functionalization with PFDT *via* immersing the Ag-layer coated Ag polyhedra anchored Si substrates in 0.05 M PFDT ethanolic solution for overnight. The substrates were removed from the PFDT solution and rinsed with copious ethanol, and dried using nitrogen gas. The as-prepared substrates were finally storied in nitrogen box for further use.

Fabrication of superhydrophobic silica bead array. The superhydrophobic silica bead array was fabricated by firstly submerging the Si wafer into silica bead (size, 103 nm) colloidal solution for 0.5hrs. The Si wafer was then removed from the colloidal solution and dried under blowing with nitrogen gas. Such silica bead deposited Si wafer were then coated with 25 nm Ag layer *via* thermal evaporation followed by functionalization with PFDT using the same method as above mentioned.

Contact angle measurements. Static contact angles were measured by drop casting a sessile droplet of 4 µL water droplet onto the platform. All contact angle measurements were repeated at least 5 times at different locations of the substrates.

Hyperspectral SERS intensity distribution map. The SERS spectra was collected by using a laser beam with an excitation wavelength of 532 nm and laser power of 0.2 mW with spectral

acquisition time of 1 s. The standard deviation of the measured SERS signal in 200 μm × 200 μm (area of the SERS map) is estimated to be 4.5 %, indicating the good homogeneity and reproducibility.

Analyte concentrating effect. Silica beads were used to determine the analyte concentrating effect and were synthesized using a modified Stober process.[49] 1 μL silica beads suspension was deposited onto a superhydrophobic platform and O_2 plasma treatment (hydrophilic) platform and allowed to dry. The area of dried spots was then characterized through digital camera and SEM. The spot areas on both superhydrophobic and hydrophilic surfaces were measured using ImageJ software.

Determining analytical enhancement factors (AEFs). AEFs were quantified using $AEF = [(I_{SERS})/(I_{Raman})] \times [(C_{Raman})/(C_{SERS})]$, where I_{SERS} and I_{Raman} were the signals recorded on SERS and normal Raman platforms, whereas C_{SERS} and C_{Raman} are the corresponding analyte concentrations measured using superhydrophobic platform and normal Raman platforms, respectively. We conduct this experiment by using 10 μL of MB solution at different concentration. For the normal Raman measurements, we drop cast a 10 μL of MB solution with concentration of 10^{-3} M on the Si wafer substrate. For the superhydrophobic-mirror substrate, the lowest detectable concentration of MB is 10^{-14} M. All the SERS spectra in current work are collected under dry conditions after the solvent in the droplet has fully evaporated, and the analytical enhancement factor was calculated on the basis of the intensities of the vibrational band of methylene blue at 1628 cm^{-1} of 25 spectra.

Density functional theory (DFT) simulation. The calculation on the interaction of MPBA-grafted Ag surface with pregnane and THC were carried out using the unrestricted B3LYP

exchange-correlation functional in the Gaussian 09 computational chemistry package. The 6-31g (d p) basis set was used for C, H and O. The LANL2DZ basis set was employed for Ag. The Ag surface was modeled using a reported triangle consisting of 6 Ag atoms. First, we optimize the geometry of the triangular Ag cluster, then 4-mercaptophenylboronic acid was placed on its vertex and the whole system was then relaxed with all the Ag atoms. Pregnane/THC molecule was then forming a boric ester bond with MPBA *via* hydroxy group, and the whole system was relaxed with Ag atoms fixed again.

SERS measurements for pregnane and THC. For SERS measurements of pure analytes, 10 µL of pregnane or THC solution (10^{-4} – 10^{-9} M) were respectively mixed with MPBA-functionalized AgNC (~ 0.2 mg mL^{-1}) at pH 11 for reaction. 10 µL-mixture solution was then placed on the superhydrophobic chip surface and then dried under ambient conditions. SERS spectra were then collected on the dried spot using a laser beam with an excitation wavelength of 532 nm and laser power of 0.2 mW with spectral acquisition time of 1 s.

For SERS measurements of the mixed analytes with varied pregane% (90-100%), we firstly prepared the samples by mixing pure pregnane and THC solution (0.1 mM) with varied volumes. Typically, sample containing 90 % pregnane (10 % THC) were prepared by mixing of 90 µL-pregnane (0.1 mM) with 10 µL-THC (0.1 mM) solution. Subsequently, 10 µL of the samples that contain varied pregnane% were mixed with MPBA-functionalized AgNC (~ 0.2 mg mL-1) at pH 11 for reaction. The 10 µL-mixture sample solution was then introduced on the superhydrophobic chip surface and then dried under ambient conditions. SERS spectra were then collected on the dried spot area using a laser beam with the same conditions as above.

Control experiments for glucose and fructose. For SERS measurements of control samples, 10 µL of glucose and fructose (10^{-4} M) were firstly mixed with MPBA-functionalized AgNC (~ 0.2 mg mL^{-1}) at pH 11 for reaction, respectively. The 10 µL-mixture was then placed on the superhydrophobic chip surface and then dried under ambient conditions. SERS spectra were then collected using a laser beam with an excitation wavelength of 532 nm and laser power of 0.2 mW with spectral acquisition time of 1 s.

Preparation of artificial urine. Artificial urine was prepared by dissolving urea (24.2 g), sodium chloride (10.0 g), monopotassium phosphate (6.0 g), and sodium phosphate (6.4 g) in 100 mL DI water.

Preparation of calibration curve. We prepared a series of urine sample with various percentage of pregnane in the range of 90-100 % by mixing pregnane and THC solution of same concentration with calculated respect volume. For instance, we prepared the urine samples which containing 90% pregnane and 10% THC by mixing 90 µL-pregnane (0.1 mM) with 10 µL-THC (0.1 mM) solution. The control samples we will replace the pregnane and THC with 10 µL of pure H_2O.

Patient recruitment. Patients presenting at the KK Women's and Children's Hospital (KKH) Singapore, 24-h Women's Clinic were recruited. Inclusion criteria were (i) patients with a single intrauterine pregnancy between 6 and 10 weeks of gestation (confirmed and dated by ultrasonography) and (ii) patients presenting with pregnancy-related per vaginam bleeding. Women with previous episodes of per vaginam bleeding or women treated with progesterone for previous per vaginam bleeding in the current pregnancy, or women diagnosed with inevitable

miscarriage, missed miscarriage, blighted ovum or women who are planning to terminate the pregnancy were excluded. Urine samples were collected at presentation for metabolite analysis.

Sample pre-treatment for artificial urine and patient urine samples. Artificial urine was spiked with different pregnane% to establish our calibration curve. Prior to reaction with MPBA-functionalized Ag nanocubes, the spiked artificial urine was desalted and purified with ZIPTIP. After reaction with the functionalized nanocubes, the mixture was further treated and purified prior to drop casting on the superhydrophobic chip for SERS measurements. A minimum of three individual samples was drop casted on the chip to obtain an average reading. This protocol was also extended to patient urine samples with minor modifications, using urine collected from non-pregnant patients to establish the baseline for pregnane and THC levels. A total of 40 patient samples were measured, where 25 measurements were done in each patient sample.

Time breakdown of detection process. The whole screening procedure significantly decreases the time required to 30 minutes, including 3 minutes for urine pretreatment, 25 minutes for drying the sample on our SPHB-mirror platform, and 2 minutes for measurement and chemometric analysis.

Chemometric analyses. Principal component analysis (PCA) was conducted using Panorama software ((LabCognition, Analytical Software GmbH & Co. KG; minimum of 25 spectra of each sample are collected from the single droplet). PCA reduces data dimensionality and converts the original variables into a set of uncorrelated linear combination of principal components (PC); PC1 typically includes the greatest variance from the orthogonal linear transformation, and PC2 includes the second greatest variance. 25 individual raw SERS spectra from 3 groups, MPBA and those coordinated with pregnane and THC respectively (total of 75 spectra), were loaded together

into the Panorama software. Standard normal variate correction and Savitzky-Golay derivative algorithm were applied to reduce spectral noise and eliminate interference from the background signals. The entire spectral range measured experimentally was selected for analysis, and a suitable number of loading vectors were employed to provide the minimum root-mean-square error for cross validation (RMSECV). In our experiment, we selected the whole spectral range with two PCs applied, which enabled spectral identification with accuracy of at least 98 %. A similar clustering process was applied for two patient urine samples, one with spontaneous miscarriage (M1) and another with ongoing stable pregnancy (S1). Partial least square analysis (PLS) was used to establish a standard calibration curve for detection in multiple scenarios, including pure analytes, multiplexed pure analytes, and multiplexed analytes in artificial urine, as well as analytes in real patient urine samples. For detection using pure analytes, 25 spectra were input for each concentration measured. For other cases, quantification model was built up by PLS using spectra collected from 90%-100% of pregnane spiked in artificial urine and patient urine samples, respectively.

Characterization. Scanning electron microscope (SEM) imaging was performed using a JEOL-JSM-7600F microscope at an accelerating voltage of 5 kV. UV-vis spectroscopic measurements were performed with a Cary 60 UV-Vis spectrometer. Zeta potential measurements were conducted using ZETASIZER NANO with DTS1070 folded capillary cell. Thermal evaporation of Ag was performed using Syskey thermal evaporator (Taiwan). Roughness of the sample was measured using JPK Nanowizard3 BioScience atomic force microscopy (AFM) on a Zeiss inverted microscope. Contact angles were measured using a Theta Lite tensiometer equipped with a Firewire digital camera and Attention from Biolin Scientific with sessile 4 μL ultrapure water droplet. Advancing and receding contact angles were determined using drop shape analysis

routine of a growing and shrinking water droplet. Each type of contact angle measurement was performed at least five times across each platform to obtain an average wetting angle. x-y SERS measurements were performed with Ramantouch microspectrometer (Nanophoton Inc, Osaka, Japan) at an excitation laser wavelength of 532 nm (power = 0.2 mW). A 20 × (N.A., 0.45) objective lens with 1 s accumulation time was used for data collection with Raman shift ranging from 500 cm^{-1} to 1600 cm^{-1}. All SERS spectra were obtained by averaging at least 25 individual spectra per Raman image.

Supporting information. This material is available free of charge *via* the Internet at http://pubs.acs.org. Supporting figures, supporting discussion, and detailed characterization of Ag nanocubes and octahedra, SPHB and control substrates, binary Ag nanoparticles monolayer fabricated *via* electrostatic assembly, surface roughness and concentration effect of optimal SPHB, SEM images of optimal substrate, working principal of SPHB substrate, analytical enhancement factor study, SERS vibrational modes and band assignments, SERS spectra of MPBA-bonded analytes, UV-vis absorption spectra of the 4MPBA binding with analytes, chemometric study of SERS spectra, SERS spectra for spiked urine.

Author Information

Corresponding authors

*Associate Professor Xing Yi Ling

E-mail: xyling@ntu.edu.sg

*Associate Professor Nguan Soon Tan

E-mail: NSTan@ntu.edu.sg

Author contributions

Y.-C. Kao, X. Han, Y.H. Lee, H.K. Lee, N.S. Tan and X.Y. Ling designed research; Y.-C. Kao, X.H., C.L.L., H.Y.F.S. performed research; C.W. Ku and T.C. Tan collected urine samples; Y.-C. Kao, X. Han, H.K. Lee, Y.H. Lee, G.C. Phang-Quang., H.Y.F. Sim and X.Y. Ling analyzed data and wrote the manuscript. All authors read and commented on the manuscript.

Acknowledgment

Funding: X.Y. Ling thanks the financial support from Singapore Ministry of Education, Tier 1 (RG11/18) and Tier 2 (MOE2016-T2-1-043) grants, and Max Planck Institute-Nanyang Technological University Joint Lab. C.W. Ku, T.C. Tan and N.S. Tan thank the financial support from the Ministry of Health Singapore Industry Alignment Fund grant (MOHIAFCat1-11010). Y.-C. Kao and C.L. Lay thank scholarship support from A*STAR, Singapore. G.C Phan-Quang acknowledges scholarship support from Nanyang Technological University, Singapore. We wish to thank all the families who participated in our research.

References

1. Khaing, M. K.; Guo, Oo, Y.; Reddy, K.; Liu, J.; Fan, X. Ultrasensitive Vapor Detection with Surface-Enhanced Raman Scattering-Active Gold Nanoparticle Immobilized Flow-Through Multihole Capillaries. *Anal. Chem*. **2012**, *84*, 3376–3381.

2. Sarpkaya, I.; Zhang, Z.; Walden-Newman, W.; Wang, X.; Hone, J.; Wong, C. W.; Strauf, S. Prolonged Spontaneous Emission and Dephasing of Localized Excitons in Air-Bridged Carbon Nanotubes. *Nat. Commun*. **2013**, *4*, 2152.

3. Langer, J.; Jimenez De Aberasturi, D.; Aizpurua, J.; Alvarez-Puebla, R. A.; Auguié, B.; Baumberg, J. J.; Bazan, G. C.; Bell, S. E. J.; Boisen, A.; Brolo, A. G.; J. Choo; Cialla-May, D.; Deckert, V.; Fabris, L.; Faulds, K.; Garcia de Abajo, F. J.; Goodacre, R.; Graham, D.; Haes, A. J.; Haynes, C. L. *et al*. Present and Future of Surface-Enhanced Raman Scattering. *ACS Nano*, **2020**, *14*, 28–117.

4. Joseph, M. M.; Narayanan, N.; Nair, J. B.; Karunakaran, V.; Ramya, A. N.; Sujai, PT.; Saranya, G.; Arya, J. S.; Vijayan, V. M.; Maiti, K. K. Exploring the Margins of SERS in Practical Domain: An Emerging Diagnostic Modality for Modern Biomedical Applications. *Biomaterials*, **2018**, *181*, 140–181.

5. Vendrell, M.; Maiti, K. K.; Dhaliwal, K.; Chang, Y.-T. Surface-Enhanced Raman Scattering in Cancer Detection and Imaging. *Trends Biotechnol.* **2013**, *31*, 249–257.

6. Knoll, W., Interfaces and Thin Films as Seen by Bound Electromagnetic Waves. *Annu. Rev. Phys. Chem.* **1998**, *49*, 569–638.

7. Ko, H.; Singamaneni, S.; Tsukruk, V. V. Nanostructured Surfaces and Assemblies as SERS Media. *Small* **2008**, *4*, 1576–1599.

8. Wang, Z.; Zong, S.; Wu, L.; Zhu, D.; Cui, Y. SERS-Activated Platforms for Immunoassay: Probes, Encoding Methods, and Applications. *Chem. Rev.* **2017**, *117*, 7910–7963.

9. Tran, V.; Walkenfort, B.; König, M.; Salehi, M.; Schlücker, S. Rapid, Quantitative, and Ultrasensitive Point-of-Care Testing: A Portable SERS Reader for Lateral Flow Assays in Clinical Chemistry. *Angew. Chem. Int. Ed.* **2019**, *58*, 442–446.

10. Alvarez-Puebla, R. A.; Liz-Marzán, L. M. SERS-Based Diagnosis and Biodetection. *Small* **2010**, *6*, 604–610.

11. Jarvis, R. M.; Goodacre, R. Characterisation and Identification of Bacteria Using SERS. *Chem. Soc. Rev.* **2008**, *37*, 931.

12. Le Ru, E. C.; Blackie, E.; Meyer, M.; Etchegoin, P. G. Surface Enhanced Raman Scattering Enhancement Factors: A Comprehensive Study. *J. Phys. Chem. C* **2007**, *111*, 13794–13803.

13. Angelis, F. D.; Gentile, F.; Mecarini, F.; Das, G.; Moretti, M.; Candeloro, P.; Coluccio, M. L.; Cojoc, G.; Accardo, A.; Liberale, C.; Zaccaria, R. P.; Perozziello, G.; Tirinato, L.; Toma, A.; Cuda, G.; Cingolani, R.; Fabrizio, E. D. Breaking the Diffusion Limit with Super-Hydrophobic Delivery of Molecules to Plasmonic Nanofocusing SERS Structures. *Nat. Photonics* **2011**, *5*, 682.

14. Li, X.; Lee, H. K.; Phang, I. Y.; Lee, C. K.; Ling, X. Y. Superhydrophobic-Oleophobic Ag Nanowire Platform: An Analyte-Concentrating and Quantitative Aqueous and Organic Toxin Surface-Enhanced Raman Scattering Sensor. *Anal. Chem.* **2014**, *86*, 10437–10444.

15. Lee, H. K.; Lee, Y. H.; Koh, C. S. L.; Phan-Quang, G. C.; Han, X.; Lay, C. L.; Sim, H. Y. F.; Kao, Y.-C.; An, Q.; Ling, X. Y. Designing Surface-Enhanced Raman Scattering (SERS) Platforms beyond Hotspot Engineering: Emerging Opportunities in Analyte Manipulations and Hybrid Materials. *Chem. Soc. Rev.* **2019**, *48*, 731–756.

16. Mahmoud, M. A.; Tabor, C. E.; El-Sayed, M. A. Surface-Enhanced Raman Scattering Enhancement by Aggregated Silver Nanocube Monolayers Assembled by the Langmuir−Blodgett Technique at Different Surface Pressures. *J. Phys. Chem. C* **2009**, *113*, 5493–5501.

17. Su, K.-H.; Wei, Q.-H.; Zhang, X.; Mock, J. J.; Smith, D. R.; Schultz, S. Interparticle Coupling Effects on Plasmon Resonances of Nanogold Particles. *Nano Lett.* **2003**, 3, 1087–1090.

18. Veloso, A. B.; Longo, J. P. F.; Muehlmann, L. A.; Tollstadius, B. F.; Souza, P. E. N.; Azevedo, R. B.; Morais, P. C.; da Silva, S. W. SERS Investigation of Cancer Cells Treated with PDT: Quantification of Cell Survival and Follow-Up. *Sci. Rep.* **2017**, *7*, 7175.

19. Shin, H.; Jeong, H.; Park, J.; Hong, S.; Choi, Y. Correlation between Cancerous Exosomes and Protein Markers Based on Surface-Enhanced Raman Spectroscopy (SERS) and Principal Component Analysis (PCA). *ACS Sens.* **2018**, *3*, 2637–2643.

20. Zrimsek, A. B.; Chiang, N.; Mattei, M.; Zaleski, S.; McAnally, M. O.; Chapman, C. T.; Henry, A.-I.; Schatz, G. C.; Duyne, R. P. V. Single-Molecule Chemistry with Surface- and Tip-Enhanced Raman Spectroscopy. *Chem. Rev.*, **2017**, *117*, 7583–7613.

21. Lek, S. M.; Ku, C. W.; Allen Jr, J. C.; Malhotra, R.; Tan, N. S.; Østbye, T.; Tan, T. C. Validation of Serum Progesterone <35nmol/L as A Predictor of Miscarriage among Women with Threatened Miscarriage. *BMC Pregnancy Childbirth*. **2017**, *17*, 78.

22. O., AH. Hanisah, Potential Use of Single Measurement of Serum Progesterone in Detecting Early Pregnancy Failure. *Malaysian J. Pathol*, **2012**, *34*, 41–46.

23. Ku, C. W.; Allen Jr, J. C.; Lek, S. M.; Chia, M. L.; Tan, N. S.; Tan, T. C. Serum Progesterone Distribution in Normal Pregnancies Compared to Pregnancies Complicated by Threatened Miscarriage from 5 to 13 Weeks Gestation: A Prospective Cohort Study. *BMC Pregnancy Childbirth* **2018**, *18*, 360.

24. Ku, C. W.; Allen Jr, J. C.; Malhotra, R.; Chong, H. C.; Tan, N. S.; Østbye, T.; Lek, S. M.; Lie, D. How Can We Better Predict the Risk of Spontaneous Miscarriage Among Women Experiencing Threatened Miscarriage? *Gynecol. Endocrinol.* **2015**, *31*, 647–651.

25. Duan, L.; Yan, D.; Zeng, W.; Yang, X.; Wei, Q. Predictive Power Progesterone Combined with Beta Human Chorionic Gonadotropin Measurements in the Outcome of Threatened Miscarriage. *Arch. Gynecol. Obstet.* **2011**, *283*, 431–435.

26. Mol, B. W.; Lijmer, J. G.; Ankum, W. M.; Veen, F. v. d.; Bossuyt, P. M. The Accuracy of Single Serum Progesterone Measurement in the Diagnosis of Ectopic Pregnancy: A Meta-Analysis. *Hum. Reprod.* **1998**, *13*, 3220–3227.

27. Ku, C. W.; Tan, Z. W.; Lim, M. K.; Tam, Z. Y.; Lin, C. H.; Ng, S. P.; Allen, J. C.; Lek, S. M.; Tan, T. C.; Tan, N. S. Spontaneous Miscarriage in First Trimester Pregnancy is Associated with Altered Urinary Metabolite Profile. *BBA Clin.* **2017**, *8*, 48–55.

28. Lee, H. K.; Lee, Y. H.; Zhang, Q.; Phang, I. Y.; Tan, J. M. R.; Cui, Y.; Ling, X. Y. Superhydrophobic Surface-Enhanced Raman Scattering Platform Fabricated by Assembly of Ag Nanocubes for Trace Molecular Sensing. *ACS Appl. Mater. Interfaces* **2013**, *5*, 11409–11418.

29. Hu, J.; Tanabe, M.; Sato, J.; Uosaki, K.; Ikeda, K. Effects of Atomic Geometry and Electronic Structure of Platinum Surfaces on Molecular Adsorbates Studied by Gap-Mode SERS. *J. Am. Chem. Soc.* **2014**, *136*, 10299–10307.

30. Benz, F.; Chikkaraddy, R.; Salmon, A.; Ohadi, H.; Nijs, B. d.; Mertens, J.; Carnegie, C.; Bowman, R. W.; Baumberg, J. J. SERS of Individual Nanoparticles on a Mirror: Size Does Matter, but So Does Shape. *J. Phys. Chem. Lett.* **2016**, *7*, 2264–2269.

31. Liu, H.; Yang, Z.; Meng, L.; Sun, Y.; Wang, J.; Yang, L.; Liu, J.; Tian, Z. Three-Dimensional and Time-Ordered Surface-Enhanced Raman Scattering Hotspot Matrix. *J. Am. Chem. Soc.* **2014**, *136*, 5332–5341.

32. Yang, D.; Afroosheh, S.; Lee, J. O.; Cho, H.; Kumar, S.; Siddique, R. H.; Narasimhan, V.; Yoon, Y.-Z.; Zayak, A. T.; Choo, H. Glucose Sensing Using Surface-Enhanced Raman-Mode Constraining. *Anal. Chem*. **2018**, *90*, 14269–14278.

33. Wang, Q.; Yang, L.; Yang, X.; Wang, K.; Liu, J. Use of Mercaptophenylboronic Acid Functionalized Gold Nanoparticles in A Sensitive and Selective Dynamic Light Scattering Assay for Glucose Detection in Serum. *Analyst*, **2013**,*138*, 5146–5150.

34. Sun, F.; Bai, T.; Zhang, L.; Ella-Menye, J.-R.; Liu, S.; Nowinski, A. K.; Jiang, S.; Yu, Q. Sensitive and Fast Detection of Fructose in Complex Media *via* Symmetry Breaking and Signal Amplification Using Surface-Enhanced Raman Spectroscopy. *Anal. Chem.* **2014**, *86*, 2387–2394.

35. Pearson, B.; Wang, P.; Mills, A.; Pang, S.; McLandsborough, L.; He, L. Innovative Sandwich Assay with Dual Optical and SERS Sensing Mechanisms for Bacterial Detection. *Anal. Methods*, **2017**, *9*, 4732–4739.

36. Yuan, K.; Mei, Q.; Guo, X.; Xu, Y.; Yang, D.; Sánchez, B. J.; Sheng, B.; Liu, C.; Hu, Z.; Yu, G.; Ma, H.; Gao, H.; Haisch, C.; Niessner, R.; Jiang, Z.; Zhou, H. Antimicrobial Peptide Based Magnetic Recognition Elements and Au@Ag-GO SERS Tags with Stable Internal Standards: A Three in One Biosensor for Isolation, Discrimination and Killing of Multiple Bacteria in Whole Blood. *Chem. Sci.*, **2018**, *9*, 8781–8795.

37. Wang, H.; Zhou, Y.; Jiang, X.; Sun, B.; Zhu, Y.; Wang, H.; Su, Y.; He, Y. Simultaneous Capture, Detection, and Inactivation of Bacteria As Enabled by A Surface-Enhanced Raman Scattering Multifunctional Chip. *Angew. Chem. Int. Ed.*, **2015**, *54*, 5132–5136.

38. Ma, R.; Hu, J.; Cai, Z.; Ju, H. Facile Synthesis of Boronic Acid-Functionalized Magnetic Carbon Nanotubes for Highly Specific Enrichment of Glycopeptides. *Nanoscale.* **2014**, *6*, 3150–3156.

39. Moeinian, A. A.; Gür, F. N.; Gonzalez-Torres, J.; Zhou, L.; Murugesan, V. D.; Dashtestani, A. D.; Guo, H.; Schmidt, T. L.; Strehle, S. Highly Localized SERS Measurements Using Single Silicon Nanowires Decorated with DNA Origami-Based SERS Probe. *Nano Lett.* **2019**, *19*, 1061–1066.

40. Haldavnekar, R.; Venkatakrishnan, K.; Tan, B. Non Plasmonic Semiconductor Quantum SERS Probe as a Pathway for *In Vitro* Cancer Detection. *Nat. Commun.* **2018**, *9*, 3065.

41. Sun, F.; Bai, T.; Zhang, L.; Ella-Menye, J.-R.; Liu, S.; Nowinski, A. K.; Jiang, S.; Yu, Q. Sensitive and Fast Detection of Fructose in Complex Media *via* Symmetry Breaking and Signal Amplification Using Surface-Enhanced Raman Spectroscopy. *Anal Chem.* **2014**, *86*, 2387–2394.

42. Li, S.; Zhou, Q.; Chu, W.; Zhao, W.; Zheng, J. Surface-Enhanced Raman Scattering Behaviour of 4-Mercaptophenyl Boronic Acid on Assembled Silver Nanoparticles. *Phys. Chem. Chem. Phys.* **2015**, *17*, 17638–17645.

43. Szafranski, C. A.; Tanner, W.; Laibinis, P. E.; Garrell, R. L. Surface-Enhanced Raman Spectroscopy of Aromatic Thiols and Disulfides on Gold Electrodes. *Langmuir* **1998**, *14*, 3570–3579.

44 Abdi, H.; Williams, L. J. Principal Component Analysis. *WIREs Comp. Stats.* **2010**, *2*, 433–459.

45. Brereton, R. G.; Lloyd, G. R. Partial Least Squares Discriminant Analysis: Taking the Magic Away. *J. Chemom.* **2014**, *28*, 213–225.

46. Chubatyi, N. D.; Pagnotti, V. S.; Bentzley, C. M.; McEwen, C. N. High Sensitivity Steroid Analysis Using Liquid Chromatography/Solvent-Assisted Inlet Ionization Mass Spectrometry. *Rapid Commun. Mass Spectrom.* **2012**, *26*, 887–892.

47. Pluskal, M. G. Microscale Sample Preparation. *Nat. Biotechnol.* **2000**, 18, 104.

48. Tao, A.; Sinsermsuksakul, P.; Yang, P. D. Polyhedral Silver Nanocrystals with Distinct Scattering Signatures. *Angew. Chem. Int. Ed.* **2006**, *45*, 4597–4601.

49. Kobayashi, Y.; Katakami, H.; Mine, E.; Nagao, D.; Konno, M.; Liz-Marzán, L. M. Silica Coating of Silver Nanoparticles Using a Modified Stöber Method. *J. Colloid Interface Sci.* **2005**, *283*, 392–396.

For table of contents only